A Reliable OFDM based MMW Mobile Fronthaul with DSP-aided Sub-band Spreading and Time-Confined Windowing

You-Wei Chen*, Shuyi Shen, Qi Zhou, Shuang Yao, Rui Zhang, Shahmeer Omar, and Gee-Kung Chang, Fellow, IEEE, Fellow, OSA

***Abstract*—Performance of digital signal processing (DSP) aided sub-band spreading orthogonal frequency division multiplexing (S-OFDM) implemented with the well-defined, time-located window is evaluated and compared with the cyclic prefix (CP) OFDM signal under severe interference circumstances. A 4-QAM mobile fronthaul over 20 km fiber link and 1 m millimeter wave (MMW) 60-GHz wireless channel is demonstrated experimentally. The bit-error rate performance of applying time windowing on OFDM and S-OFDM are measured in the single channel scenario. In such simplified system, CP-OFDM is found to be a widely adopted waveform. While, as it suffers from the unexpected external interference, the received error vector magnitude (EVM) would be degraded dramatically for typical OFDM signals. By applying the Hanning window, the impact on the EVM performance can be alleviated as the interference is at the edge of the desired signal band and resulting a 2.5% EVM enhancement. However, an irrecoverable 20% data loss is obtained if the interference is totally immersed in the victim signal. In contrast, S-OFDM exhibits a frequency diversity property by grouping OFDM subcarriers into several sub-bands and spreading them into whole available bandwidth. Thus, as S-OFDM suffers from strong interference inside the signal band, about 12.61% and 43.53% EVM improvements of the average and the worst subcarrier performance with respect to the ordinary OFDM can be achieved via applying the spreading codes orthogonality restoring equalizer (ORE). All subcarriers in the S-OFDM are generated to meet the forward error correction (FEC) threshold with reasonably flat performance. Therefore, the S-OFDM shows its superiority in an MMW mobile fronthaul for better reliability in data transmission.**

***Index Terms*—Digital signal processing, Mobile fronthaul, orthogonal frequency division multiplexing.**

I. Introduction

TO satisfy the rapidly growing demand of mobile service requirements, orthogonal frequency division multiplexing (OFDM) based fiber-wireless networking technologies (FiWIN) [1-4] attracts tremendous interest because its inherent benefits of high spectral efficiency and robustness against to fiber dispersion. Meanwhile, by exploring higher frequency to the millimeter wave (MMW) band, i.e., 30-300 GHz [5-10] and simplifying the hardware of remote radio units (RRUs), FiWIN facilitates an ultra-dense small cell deployment [11,12] for increasing the geographical throughput for the next generation mobile fronthaul. However, as massively deploying of mobile cells, the wireless environment becomes much complex. Since we cannot always guarantee conducting a perfect interference management [13-15] and considering that some of small cells may being modified, ageing, or failing, new challenges are incurred for FiWIN, i.e., unexpected interference will cause a significant performance issue. For instance, it is possible that a desired data from a nearby small cell transmitter is affected by a micro cell signal transmitted in the same or near edge of the frequency band because of errors in the frequency settings or dis-coordinating from other service carriers. Receiver may also be overwhelmed by the co-channel black-reflection uplink in a bi-directional radio system, as depicted in Fig. 1. With a series processing of interference identifying, fixing and resolving, the interference can be eliminated in a time-consuming method, but subscribers would suffer a drop in quality of service during that period. On the other hand, for a wireless full-duplexing system, the residual self-interference is another in-band impairment source with around 10 dB power lower than the signal of interest even after applying interference cancellation technique [16].

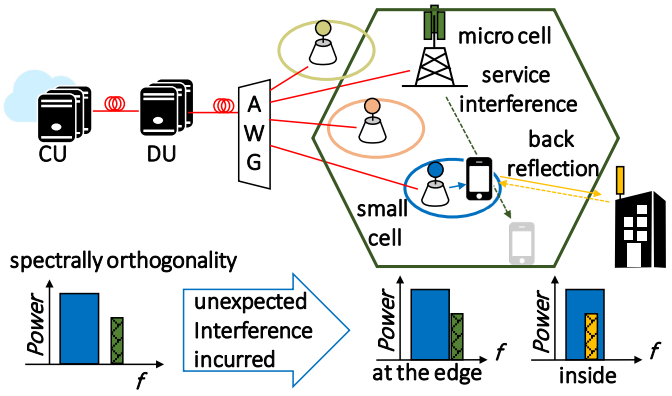

Fig. 1. Conceptual diagram of an OFDM based fiber-wireless integrated MMW mobile fronthaul suffering from unexpected interference.

This manuscript received XXXX; accepted XXXX. Date of publication XXXX; date of current version XXXX.

Y.-W. Chen, S. Shen, Q. Zhou, S. Yao, R. Zhang, S. Omar, and G.-K. Chang are with the School of Electrical and Computer Engineering, Georgia Institute of Technology, Atlanta, GA 30308, USA.
(yu-wei.chen@ece.gatech.edu)

This project is in part supported by an NSF innovation program grant for I/UCRC Center of Fiber Wireless Integration and Networking.

Mitigation of undesired interference in multi-carrier transmission system without causing service interruption to the users during the interference resolving period is a very important fiber-wireless networking technology for efficient mobile fronthaul in New Radio access architecture. A conventional solution to this problem is to incorporate extra backup data block. Therefore, mobile fronthaul utilizing the adaptive diversity combining [17] and the coordinated mapping and combining [18] techniques were proposed at an expense of sacrificing the precious spectrum resource to enhance the system reliability. On the other hand, OFDM with digital signal processing (DSP) aided sub-band spreading has been proposed to mitigate the transmission distance dependent loss due to radio frequency (RF) selective power fading [19] in passive optical networks. By grouping subcarriers of OFDM into to several sub-bands and spreading them into whole operated bandwidth, the received performance could be enhanced without any pre-knowledge of the RF power fading locations. The sub-band spreading-OFDM (S-OFDM) inherently gains the advantage from the standard OFDM and exhibits beneficial features, such as high spectral efficiency and tolerance to inter-symbol interference (ISI). Meanwhile, by exploiting its frequency diversity property, it is relatively insensitive to frequency domain impairments and thus provides a potential solution for mitigating unexpected external interference in the frequency domain for mobile fronthaul.

Furthermore, multicarrier signal based on rectangular pulse in time domain is suffering from various frequency domain impairments, such as high out-of-band (OOB) noise due to the infinite tails formed by the sinc-function subcarriers spectra. To improve the frequency localization for desired signals, filter bank multicarrier (FBMC) [20,21] designed with per-subcarrier filters or universal filtered multicarrier (UFMC) [22,23] with sub-band filters were widely studied for reducing OOB and inter-carrier interference (ICI) from nearby carrier signals. However, in order to implement a faster spectral roll-off filter, its time response would be longer and requiring a longer symbol duration, which reduce the overall throughput. Meanwhile, the frequency filters would increase the complexity of the transmitter and receiver design, which opposes to the cost-sensitive RRUs for the next generation mobile fronthaul. Thus, an alternative method to reduce the OOB is proposed by conducting a time domain windowing. Weighted-overlap-add (WOLA) OFDM [24,25] introduced by Qualcomm has a lower implementation complexity than the frequency domain filtering. However, it requires an additional time overhead beyond cyclic prefix (CP) length. To keep the same symbol duration as the conventional CP-OFDM, the well-time-located short perfect reconstruction time window [26-28] for multicarrier systems was explored. Nevertheless, the effects of combining S-OFDM and time-confined windowing in conjunction with unexpected external interference in an MMW mobile fronthaul has not been studied.

In this work, in order to reduce the unexpected frequency domain impairments, the received signal power performance of OFDM and S-OFDM in combination with the time-confined window are investigated. In addition to implementing one-tap zero-forcing (ZF) equalizer, S-OFDM with minimum mean squared error (MMSE) based coding channel orthogonality restoring equalizer (ORE) [19] is also employed for realizing the frequency diversity gain. The principle of time and frequency domain localization of the applied time domain window are presented here. The single channel bit-error ratio (BER) performance with and without windowing are firstly characterized in term of the received optical power in back-to-back and 20-km fiber link as well as 1-m wireless MMW transmission. The suppression on the interference induced impairments are extracted from the analysis of the average error vector magnitude (EVM) in the case of 20-km fiber transmissions. The improvements among subcarriers for both OFDM and S-OFDM with ZF and ORE are discussed and compared. The time-confined windowing offers a better frequency localization and relaxes the subcarrier degradation at the desired signal spectrum edge in more complex and massive machine-type services as well as in the densified small cell environment. While, S-OFDM explores the frequency diversity and exhibits a superior EVM performance over the OFDM scheme especially encountering an unexpected interference.

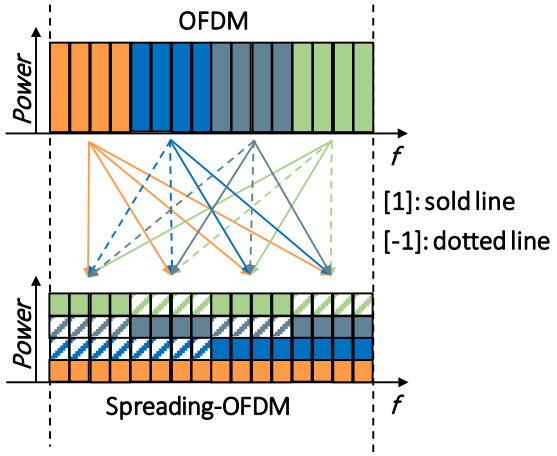

Fig. 2. Conceptual diagram of frequency spreading process of S-OFDM from typically OFDM data with OVSF code length equal to 4.

II. Operation Principles

Figure 2 illustrates a conceptual diagram of the DSP-aided sub-band S-OFDM encoding process. To generate S-OFDM, firstly we have to divide M subcarriers from the conventional OFDM into N sub-band, in each of them has M/N subcarriers. The spreading code employed in this demonstration is the orthogonal variable spreading factor (OVSF) code [29] with its code length equivalent to the N. The subcarrier data is copied and multiplies by the dedicated OVSF codes. Therefore, the frequency domain output of S-OFDM signal in a single symbol duration can be expressed as [19]

$$\mathrm{S}[i] = \sum_{n=1}^{N} d_{q,n} C_n[i],\ i = 1,2...,M \tag{1}$$

where i is the output subcarrier index, $d_{q,n}$ is the nth coding channel data, which is originated form ordinary OFDM with its subcarrier index of $q=l,l+1\ldots,l+M/N-1$, $l=(n-1)(M/N)+1$, and C_n is the nth OVSF code with its length extended to M. An example with M=16 and N=4 is shown in Fig. 2, the code word

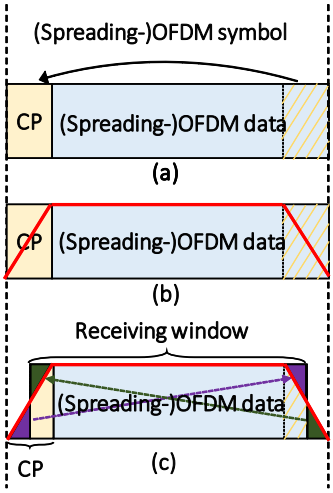

Fig. 3. Conceptual diagram of modified time-confined windowing process. (a) Ordinary CP-OFDM data. (b) Desired data with Hanning window weighted. (c) CP-folding at the receiver-end for windowing signals.

equal to 1 is represented by the sold line, and -1 is shown by the dotted line. After codes assignment, each sub-band data is spread into the whole available bandwidth and aggregated as the data throughout, which results the same transmitted bandwidth and capacity as the ordinary OFDM. It is worth to mention that lengthening the code length of OVSF could carry out more frequency diversity [19]; however, to keep the low-complexity nature of receiver at RRUs, we will divide OFDM subcarriers into 4 sub-bands in this demonstration.

To confine the frequency domain location and concurrently preserve the time domain symbol duration, the time-confined Hanning windowing is conducted here and given by [20,30]

$$w(k)=\begin{cases}0.5(1-\cos(2\pi\dfrac{k-1}{\Delta})), & if\ 1\le k\le\Delta\\ 1, & if\ \Delta+1\le k\le L\\ 0.5(1-\cos(2\pi\dfrac{k-1}{\Delta})), & if\ L+1\le k\le W\end{cases}, \qquad (2)$$

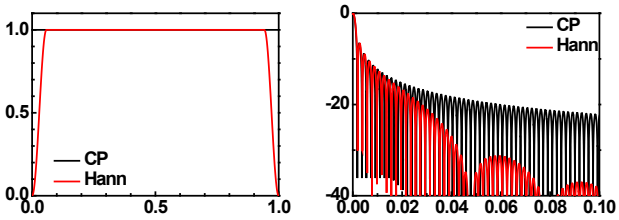

Fig. 4. (a) Time domain response of the time-confined Hanning window. (b) Frequency domain response of the Hanning window with the CP length of 1/16.

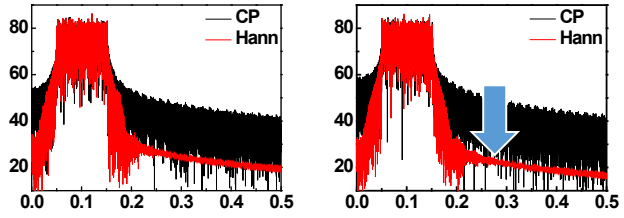

Fig. 5. The signal spectra with and without the modified Hanning window. (a) OFDM. (b) S-OFDM.

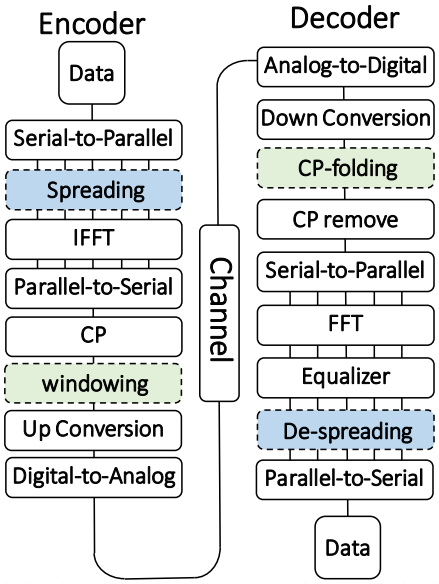

Fig. 6. Digital signal processing of S-OFDM with time windowing.

where k is the time domain index per-symbol, L and W are the (S-)OFDM data duration without and with CP, whose length is $\Delta=W-L$. Unlike normal Hanning windowing, we inset a period of constant weighting in the middle to make its length equal to the symbol duration of CP-OFDM. To perform such discrete symbol shaping, an additional step of time domain multiplying at the transmitter-side is added from traditional CP-(S-)OFDM, and thus a negligible complexity is induced. A symmetrical power weighting within CP length is achieved in the front and end of each transmitted data symbol, which is obtained by

$$\mathrm{X(k)} = IFFT\{S(k)\}w(k)\,, \qquad (3)$$

To redeem the original data, a process called CP-folding [25] is employed at the receiver-side. As indicated in Fig. 3(c), the first-half of weighted-CP is copied and added to the first-half of its counterpart at the end of the transmitted data, and vice versa.

The time and frequency domain of windowing response with the CP length of 1/16L are depicted in Fig. 4(a) and (b). It is worth to mention that the CP operation can be considering as a rectangular windowing, and thus its frequency response is a sinc function with high energy sidelobes. As one can see that a fast decline of the side-lobe power and an obvious improvement of frequency localization is achieved via the proposed Hanning window. However, its main-lobe is slightly boarded [30], which will reduce the orthogonality among subcarriers. The output spectra of OFDM and S-OFDM with and without windowing are shown in Fig. 5 in the case of 100MHz signal bandwidth and Δ/L=1/16. Since the S-OFDM only manipulating the complex data on subcarriers, its spectrum is almost identical to OFDM. While, with the Hanning window, both of OFDM and S-OFDM exhibit a remarkable OOB suppression ratio.

The encoding and decoding process of S-OFDM with time domain windowing is depicted in Fig. 6. Besides the dotted frame of spreading and windowing steps, the residual parts are identical to ordinary OFDM process, including inverse fast Fourier transform (IFFT), parallel-to-serial conversion and so on. The detailed equalization processing is specified in our previous work [19], including ZF with inner product to separate

each OVSF encoded data and the MMSE based ORE to re-establish the orthogonality among OVSF coding channel when S-OFDM is suffering from severe frequency domain impairments. The ZF equalizer, applying an inverse weighting of the frequency channel response, will inevitably amplify the unwanted interference noise under low signal-to-interference noise ratio (SINR) circumstances. Thus, if S-OFDM is restored via ZF, there is no room to execute the advantage of frequency diversity gain. To circumvent such drawback, the ORE composed of the widely-adopted MMSE equalizer [31] and a one-step iteration process, is applied to carry out the frequency diversity gain.

III. Experiment Setup

The experimental setup of the OFDM based MMW mobile fronthaul is illustrated in Fig. 7. In the transmitter-side, a tunable laser source at 1549.87 nm is employed. A polarization controller (PC) is applied for adjusting the polarization state before injecting the continuous wave laser into Mach-Zehnder modulator (MZM), which drive via a 31.6-GHz sinusoidal clock source at its null point for optical carrier suppression (OCS) [9,32]. Such manipulation requires only half of the desired frequency to modulate the MZM and therefore reduce the requirement of the high frequency electrical oscillator at the distributed unit (DU). Two separated optical carriers with 63.2 GHz are achieved with an 18-dB central carrier suppression ratio. The optical spectra before and after first step MZM are inset in Fig. 7(a) and (b). To fully utilizing the linear modulation region of the next step MZM and realize a higher signal to noise ratio (SNR) for the proposed multicarrier signals, a better carrier suppression ratio is mandatory, and therefore a 50/100 optical inter-leaver and an Erbium-doped fiber amplifier (EDFA) are embedded between two MZMs.

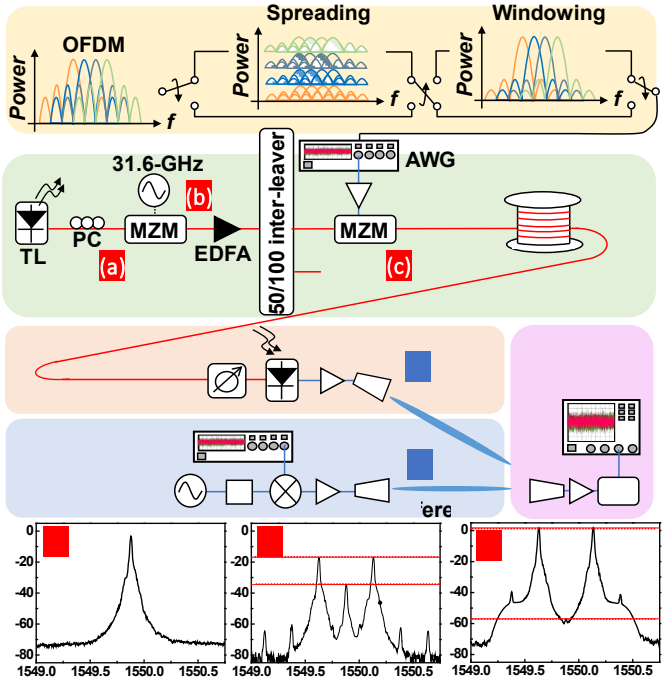

Fig. 7. Experimental setup of the proposed windowed (S-)OFDM based MMW mobile fronthaul with deliberately 20-MHz unwanted interference.

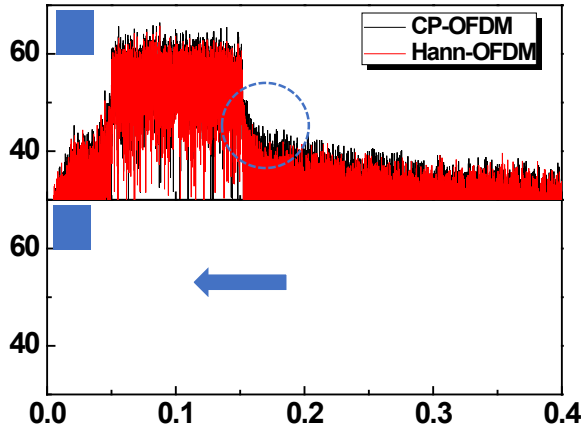

Fig. 8. (i) Electrical spectra of OFDM schemes with and without the Hanning window after 20-km fiber link and 1-m MMW wireless transmission. (ii) Interference spectra with their central frequencies intentionally shifting of 200-, 100-, and 20-MHz.

The offline Matlab is based on the typical OFDM processes as shown in Fig. 6. 4-QAM vector signal is employed here before serial-to-parallel conversion. Prior to apply Hanning window to the time domain symbols, we should conduct the frequency domain spreading for S-OFDM. 52 subcarriers are deployed over 8192 FFT size, and each sub-band has 13 (=52/4) subcarriers with OVSF code length of 4. An offline 100-MHz frequency up-conversion is applied for directly modulating the complex vector signals and simultaneously avoiding the block frequency around DC. After sampling via a 16 GSa/s arbitrary waveform generator (AWG), all the examined signals occupied about 100-MHz bandwidth. The output electrical signal is pre-amplified to reach the required peak-to-peak voltage and then fed into the linearly modulated MZM. The optical spectrum after signal modulation with 60-dB OCS ratio is inset in Fig. 7(c). The transmission distance is regulated to 20 km with the launched power of 5.2 dBm.

At RRU-side, an optical attenuator is employed for received optical power test before the signal being optical-to-electric down-converted via a 60-GHz photodetector (PD). A power amplifier (PA) with 25-dB gain and a horn antenna are used for establishing a 1-m MMW wireless transmission. To study the impairments by the unexpected spectrally interference of other service carriers or the reflection of the uplink signals. Another OFDM stream is deliberately generated via aforementioned DSP process but only occupies 20 MHz bandwidth. The central frequency setting of the unwanted interference is achieving via offline DSP and then physically 60-GHz up-converted to the MMW channel by a pair of 4-times frequency multiplier and a 15-GHz sinusoidal source.

For the subscriber receiving process, both desired signal and unwanted interference are firstly collected by the same horn antenna followed by a low-noise amplifier (LNA) with 35-dB gain. Before sampled via a 20 GSa/s real-time scope (RTS), an envelope detector (ED) with 300-MHz bandwidth is employed to down-convert the MMW signals to intermediate frequency. The electrical spectra of OFDM with and without spreading are almost the same as indicated in Fig. 5, and thus only the OFDM scheme is presented in the upper inset of Fig. 8. In contrast to

Fig. 5, one can note that only a slightly OOB suppression is observed which obscured by the noise floor and the achievable SNR is around 20 dB. Such noise floor is caused by the inherent quantization noise of the employed AWG and RTS as well as the optical and electrical amplifiers in the FiWIN system. The central frequency of the intentionally added interference is manually shifting from 200-MHz to 20-MHz to evaluate the performance degradation as the desired signals suffering from different amount of interference. The interference streams are also conducting the windowing for the corresponding signals. To not loss of the generality, the interference power is about 10 dB lower than the desired signals. The corresponding spectra of 20-, 100- and 200-MHz are depicted in Fig. 8(ii) as examples.

The decoding DSP is a reverse process of the encoding [19]. We firstly conduct hand searching, frequency down-conversion, and then CP-folding to restore the windowing data. After FFT, the signal is converted into frequency domain, we can process the channel equalization and de-spreading process. Finally, the desired signal is evaluated via its BER and EVM.

IV. Experimental Results and Discussion

As shown in Fig. 9, the received performance of the 4-QAM single channel CP-OFDM and Hann-OFDM are evaluated via two decoding processes, i.e., ZF and the MMSE based ORE in back-to-back (BtB) and after 20 km SMF transmissions. The BER performance is irrelevant to the transmission distance due to the narrow subcarrier bandwidth property of OFDM. The received sensitivities, defined as the received power satisfied the FEC criterion, i.e., BER=$3.8\text{x}10^{-3}$ [33], via ZF are -8.51 and -8.21 dBm for the CP-OFDM and Hann-OFDM, respectively. Since time domain windowing would reduce the orthogonality among subcarriers of OFDM, thus there is an around 0.3 dB received power penalty. While, by applying ORE, the received sensitivities of the two schemes of OFDM are getting improved trivially of 0.2 dB.

Figure 10 illustrates the received BER performance of single channel CP-S-OFDM and Hann-S-OFDM in BtB and over 20-km fiber link with 1-m MMW wireless transmission. As we mentioned before, since S-OFDM manipulates the complex data on the frequency domain, their subcarrier properties are

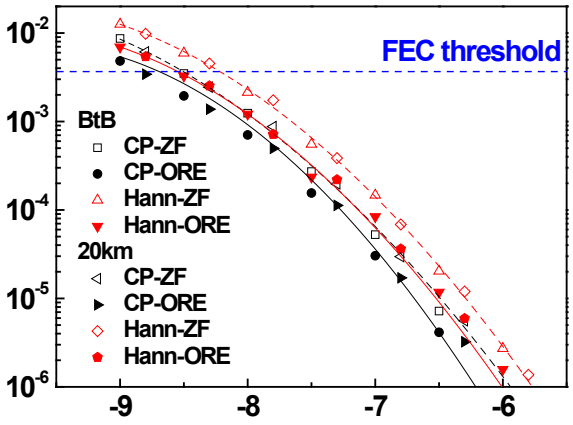

Fig. 9. Received BER of CP-OFDM and Hann-OFDM in BtB and after 20 km fiber transmission.

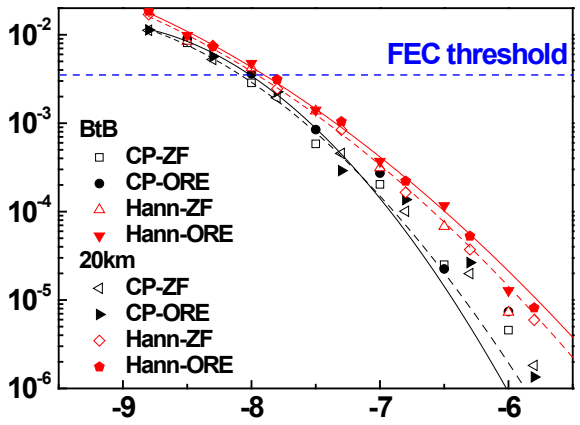

Fig. 10. Received BER of CP-S-OFDM and Hann-S-OFDM in BtB and after 20 km fiber transmission.

similar to the typical OFDM. Therefore, there is also almost no power penalty between BtB and after 20-km fiber transmission. The received sensitivities of the S-OFDM via ZF are -8.08 and -7.96 dBm with and without Hanning windowing, respectively. Again, a lightly power penalty is caused by the loss of orthogonality among S-OFDM subcarrier due to the time domain windowing. In addition, as compare to the CP-OFDM scheme, around 0.4-dB power penalty is measured as we apply DSP-aided sub-band S-OFDM signal because the signal peak-to-average ratio (PAPR) varies from 12.13 dB to 12.67 dB by the frequency spreading process. Unlike the OFDM scheme, the ORE does not enhance the received performance, since there is no room for the frequency diversity due to the single flat-response channel.

Figure 11 exhibits a comparison of OFDM and S-OFDM with and without the time-confined windowing conducted via their average EVM performance in the case of the 100-MHz transmitted bandwidth and the received optical power of 0 dBm over 20-km fiber link and 1-m MMW channel. As they are encountered the unexpected interference, whose central frequency is shifting from 200 MHz to 20 MHz, the average EVM are drastically degraded especially when they are inside

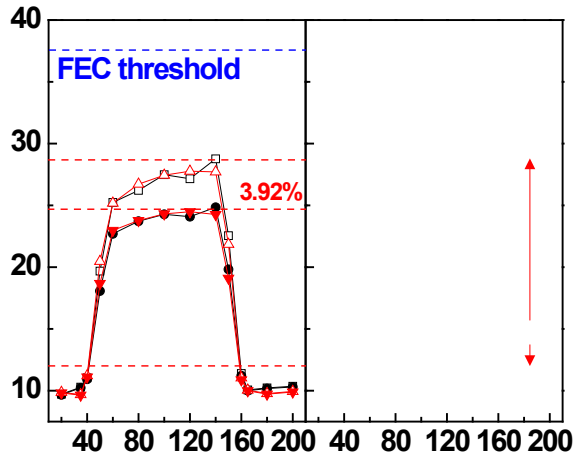

Fig. 11. Average EVM performance of OFDM and S-OFDM under strong frequency domain impairments by the shifting central frequency interference.

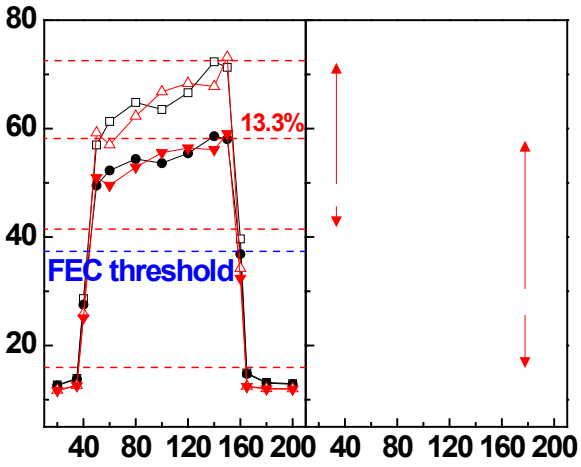

Fig. 12. The worst subcarrier EVM performance of OFDM and S-OFDM suffering from strong interference with shifting noise frequency from 200 to 20 MHz.

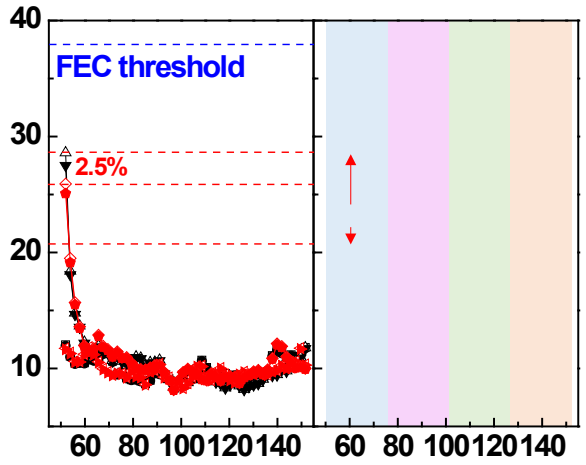

Fig. 13. EVM performance among subcarriers of OFDM and S-OFDM when the interference is located at 20- and 40-MHz central frequency.

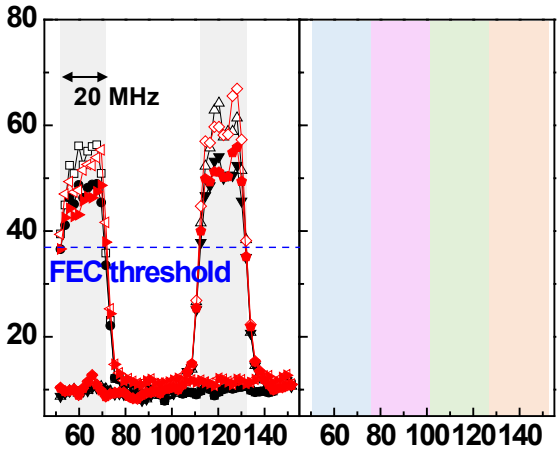

Fig. 14. EVM performance among subcarriers of OFDM and S-OFDM when the interference is located at 60- and 120-MHz central frequency.

the same frequency channel. Even the unwanted interference is outside the desired signal, it still declines the receiver sensitivity by raising the in-band noise level. Consequently, the deleterious interference becomes the dominating parameter for the received EVM, and the subcarrier orthogonality declination by the time-confined Hanning window causes a negligible performance difference for both OFDM and S-OFDM. For the OFDM scheme with ZF, the EVM drops significantly from 9.7% as interference with central frequency of 20-MHz to 28.7% as interference totally collided with the desired signal. While, ORE can circumvent amplifying the undesired noise and thus enhance the EVM performance of 3.92% for CP-OFDM and Hann-OFDM. On the other hand, DSP-aided S-OFDM with ZF performs similar to OFDM scheme. However, even the interference is inside the desired signal, a hugely EVM performance improvement of 16.53% can be achieved for sub-band S-OFDM due to the frequency diversity gain by applying ORE.

While, the average EVM performance could not accurately reveals subscribers' performance when they are suffering from the strong interference. Therefore, we further evaluate the worst subcarrier EVM of OFDM and S-OFDM. The worst subcarrier EVM performance of them are shown in Fig. 12. The worst performance of OFDM with ZF and ORE are 72.3% and 59%, respectively. Even though applying ORE can mitigate the interference amplification and improve the worst EVM of 13.3%, the EVM is still far away from the forward error correction (FEC) threshold [33]. As indicated in Fig. 8(a), the windowing can slightly improve the frequency localization in the experimental demonstration, the worst subcarrier with the Hanning window outperforms slightly than the CP-OFDM when the interference at the frequency edges of the desired signals.

On the other hand, even with ZF, the S-OFDM can average out the subcarrier performance due to frequency spreading and thus hugely enhance the EVM performance of the worst subcarrier by 30.7% as comparing the OFDM. However, there are still some of the scenarios fail to reach the FEC requirement. As applying ORE, the S-OFDM performs much better than the CP-OFDM but also Hann-OFDM signals due to the frequency diversity gain. The worst subcarrier EVM in S-OFDM scheme is 15.47%, which is 43.53% improved from the conventional OFDM with ORE.

The EVM results among subcarriers of OFDM and S-OFDM after 20 km fiber link and 1-m MMW wireless transmission are given in Fig. 13 with unwanted interference located at 20-MHz and 40-MHz central frequencies. It is clear that all subcarriers perform similar with ZF and MMSE based ORE for CP-OFDM as the interference is outside (i.e., 20-MHz) the desired signal band.

While, when the harmful interference is located at the edge of the desired signal, i.e., 40-MHz, the lowest subcarrier of the desired signal is particularly vulnerable to the impairment by the higher OOB interference. Since the Hanning window can slighting improve the frequency confinement, an enhanced EVM of 2.5% can be achieved for OFDM. On the other hand, the windowing benefit is not significant for S-OFDM since it spreads the sub-band into the whole available bandwidth. It is worth to note that since we apply spreading factor equal 4, the

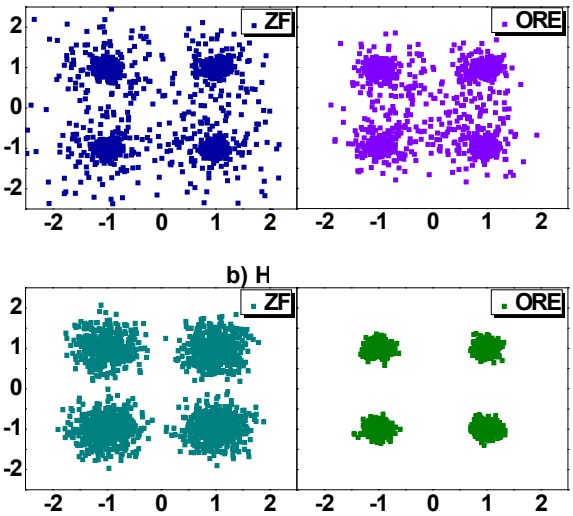

Fig. 15. Constellation diagrams of OFDM and S-OFDM with time domain Hanning window and different equalizers when they are suffering from the 120-MHz central frequency interference.

EVM could be classified into 4 groups, and each group can be considered as a minified version of OFDM. An 8.12% EVM improvement at the edge can be achieved via ZF when the interference is located at 40-MHz central frequency. Since the orthogonality among coding channels is restored by the ORE operation, the subcarrier performance of the S-OFDM is relatively insensitive to the external interference.

We also evaluate the EVM performance among subcarrier when the interference is inside the same frequency band of the desired signal, as depicted in Fig. 14. A significant performance degradation can be measured for CP-OFDM and Hann-OFDM schemes. Again, compared with applying ZF equalizer, the subcarrier suffering from the strong interference can benefit from MMSE based ORE. This can be understood because the MMSE-based equalizer could avoid the noise amplification during the DSP processing, it is more efficient for the subcarrier with a lower SINR. However, the region infected by the interference still results an unrecoverable EVM performance and cause around 20% data loss for OFDM schemes. On the other hand, even suffering from the strong interference totally overlapped with the desired signals, the performance enhancement by ORE of S-OFDM is significant and it provides an equalized and enhanced performance among subcarrier in this demonstration.

Figure 15 visualizes the advantages of the Hann-S-OFDM with respect to the Hann-OFDM by their constellation. As strong interference inside the Hann-OFDM, the constellation is spread out and ruined with ZF. They can be converged via ORE; however, they still cannot be distinguished clearly. While, by applying Hann-S-OFDM, even with the one-tap ZF, 4-QAM constellation points are achieved distinctly. With the ORE, a more concentrated constellation is obtained.

V. Conclusions

This paper presents an experimental evaluation of the OFDM and S-OFDM with and without the time-confined Hanning window in a 60-GHz MMW mobile fronthaul system over 20 km fiber and 1-m wireless transmission. A remarkable OOB suppression can be achieved via the modified Hanning window in the simulation circumstance. However, in our experimental results, the effectiveness of OOB suppression is not strong due to the quantization and amplifier spontaneous noise of the employed devices in our lab. The measured performance of both OFDM and S-OFDM shows a negligible power penalty after applying the time-confined windowing in the single channel scenario due to the orthogonality declination among subcarriers. In the presence of strong interference, such drawback becomes a negligible impairment.

For OFDM, its received power performance will be dominated by the unwanted interference residing in the same frequency band of the same receiver-frontend, which totally corrupts the subcarrier information. If the interference occurs at the edge of the desired signal band, the time-confined Hanning window can reduce the impact of interference and gain 2.5% EVM improvement. Compare to ZF, the subcarrier EVM performance can be enhanced up to 13.3% with the help of ORE when interference is immersed inside the OFDM signals. But it still fails to meet the specific FEC threshold. Such irrecoverable frequency impairment, in this case, can cause a loss of 20% transmitted data.

On the other hand, S-OFDM can provide a 30.7% EVM enhancement for the worst subcarrier with respect to OFDM scheme by applying ZF. This is due to its capability to average out the frequency domain impairments. Meanwhile, through the measurement, in the worst case, EVM performance are significantly improved by 43.53% via ORE. Even if S-OFDM suffering from the same amount of interference, it exhibits only a small performance degradation and maintains a reasonable subcarrier performance while guaranteeing all subcarrier to meet the FEC criterion. Therefore, it is a promising multicarrier waveform for archiving a high-reliability MMW mobile fronthaul.

References

[1] C. Lim, A. Nirmalathas, M. Bakaul, P. Gamage, K.-L. Lee, Y. Yang, D. Novak, and R. Waterhouse, "Fiber-wireless networks and subsystem technologies," *J. Lightw. Technol.*, vol. 28, no. 4, pp. 390-405, 2010.

[2] J. Yu, X. Li, and N. Chi, "Faster than fiber: over 100-Gb/s signal delivery in fiber wireless integration system," *Opt. Express*, vol. 21, no. 19, pp. 22885-22904, 2013.

[3] G.-K. Chang and P.-C. Peng, "Grand challenges of fiber wireless convergence for 5G mobile data communications [Invited]," in *Proc. OECC*, Jul. 2018, paper 5A4-1.

[4] R. Deng, J. Yu, J. He, M. Chen, Y. Wei, L. Zhao, Q. Zhang, and X. Xin, "Twin-SSB-OFDM transmission over heterodyne W-band fiber-wireless system with real-time implementable blind carrier recovery," *J. Lightw. Technol.*, vol. 36, no. 23, pp. 5562-5572, 2018.

[5] J. Yu, "Photonics-assisted millimeter-wave wireless communication," *IEEE J. Quantum Electron.*, vol. 53, no. 6, pp. 1-17, 2017.

[6] J. Yu, X. Li, and W. Zhou, "Tutorial: broadband fiber-wireless integration for 5G+ communication," *APL Photonics*, vol. 3, no. 11, 111101, 2018.

[7] C.-T. Tsai, C.-H. Lin, C.-T. Lin, Y.-C. Chi, and Gong-Ru Lin, "60-GHz millimeter-wave over fiber with directly modulated dual-mode laser diode," *Sci. Rep.*, vol. 6, DOI: 10.1038/srep27919, 2016.

[8] Y. Niu, Y. Li, D. Jin, L. Su, and A. V. Vasilakos, "A survey of millimeter wave communications (mmWave) for 5G: opportunities and challenges," *Wireless Netw.*, vol. 21, no. 8, pp. 2657–2676, 2015.

[9] Y. Tian, K.-L. Lee, C. Lim, and A. Nirmalathas, "60 GHz analog radio-over-fiber fronthaul investigations," *J. Lightw. Technol.*, vol. 35, no. 19, pp. 4304-4310, 2017.
[10] S. Rangan, T. S. Rappaport, and E. Erkip, "Millimeter-wave cellular wireless networks: potentials and challenges," in *Proc. IEEE*, vol. 102, no. 3, pp. 366–385, Mar. 2014.
[11] M. Ding, D. López-Pérez, H. Claussen, and M. A. Kaafar, "On the fundamental characteristics of ultra-dense small cell Networks," *IEEE Netw.*, vol. 32, no. 3, pp. 92-100, 2018.
[12] M. Xu, J.-H. Yan, J. Zhang, F. Lu, J. Wang, L. Cheng, D. Guidotti, and G.-K. Chang, "Bidirectional fiber-wireless access technology for 5G mobile spectral aggregation and cell densification," *J. Opt. Commun. Netw.*, vol. 8, no. 12, pp. B104-B110, 2016.
[13] A. L. Stolyar and H. Viswanathan, "Self-organizing dynamic fractional frequency reuse for best-effort traffic through distributed inter-cell coordination," in *Proc. INFOCOM*, pp.1287-1295, Apr. 2009.
[14] W. Nam, D. Bai, J.Lee, and I. Kang, "Advanced interference management for 5G cellular networks," *Commun. Mag.*, vol. 52, no. 5, pp. 52-60, 2014.
[15] V. Fern´andez-L´opez, K. I. Pedersen, B. Soret, J.Steiner, and P. Mogensen, "Improving dense network performance through centralized scheduling and interference coordination," *Trans. Veh. Technol.*, vol. 66, no. 5, pp. 4371-4382, 2017.
[16] Q. Zhou, J. Ge, and M. P. Fok, "Fast dynamic in-band RF self-interference cancellation for enabling efficient spectral usage," in *Proc. OFC*, Mar. 2017, paper W4B.5.
[17] F. Lu, M. Xu, S. Shen, Y. M. Alfadhli, H. J. Cho, and G.-K. Chang, "Demonstration of inter-dimensional adaptive diversity combining and repetition coding in converged MMW/FSO links for 5G and beyond mobile fronthaul," in *Proc. OFC*, Mar. 2018, paper M3K.4.
[18] R. Zhang, F. Lu, M. Xu, S. Liu, P.-C. Peng, S. Shen, J. He, H. J. Cho, Q. Zhou, S. Yao, and G.-K. Chang, "An ultra-reliable MMW/FSO A-RoF system based on coordinated mapping and combining technique for 5G and beyond mobile fronthaul," *J. Lightw. Technol.*, vol. 36, no. 20, pp. 4952-4959, 2018.
[19] Y.-W. Chen, Y.-C. Chi, H.-Y. Wang, C.-T. Tsai, Z.-K. Weng, K.-M. Feng, and G.-R. Lin, "Constructed MC-CDMA LR-PON with colorless laser diode and multicode interference cancellation DSP," *J. Lightw. Technol.*, vol. 35, no. 13, pp. 2646-2653, 2017.
[20] B. Farhang-Boroujeny, "OFDM versus filter bank multicarrier," *Signal Process. Mag.*, vol. 28, no. 3, pp. 92-112, 2011.
[21] Y. Liu, X. Chen, Z. Zhong, B. Ai, D. Miao, Z. Zhao, J. Sun, Y. Teng, and H. Guan, "Waveform design for 5G networks: analysis and comparison," *IEEE Access*, vol. 5, pp. 19282-19292, 2017.
[22] F. Schaich, and T. Wild, "Waveform contenders for 5G - OFDM vs. FBMC vs. UFMC," in *Proc. ISCCSP*, pp. 457-460, Aug. 2014.
[23] T. Wild, F. Schaich, and Y. Chen, "5G Air Interface Design based on Universal Filtered (UF-)OFDM," in *Proc. Int. Conf. Digit. Signal Process.*, pp. 20-23, Aug. 2014.
[24] Qualcomm Technologies, "5G waveform & multiple access techniques," Nov. 2015.
[25] R. Zayani, Y. Medjahdi, H. Shaiek, and D. Roviras, "WOLA-OFDM: A potential candidate for asynchronous 5G," in *Proc. GC Wkshps*, pp. 1-5, Dec. 2016.
[26] T. Kanesan, S. T. Le, D. Roque, and A. D. Ellis, "Non-rectangular perfect reconstruction pulse shaping based ICI reduction in CO-OFDM," *Opt. Express*, vol. 22, no. 2, pp. 1749-1759, 2014.
[27] S. Shen, T. Kanesan, F. Lu, M. Xu, L. Cheng, J. Wang, Y. M Alfadhli, H. J. Cho, S. M. Mitani, and G.-K. Chang, "Efficient mobile fronthaul using windowed OFDM exhibiting high CFO tolerance and strong OOB-leakage suppression with low DSP complexity," in *Proc. OFC*, Mar. 2018, paper Th3G.7.
[28] D. Pinchon and P. Siohan, "Closed-Form Expressions of Optimal Short PR FMT Prototype Filters," in *Proc. GLOBECOM*, pp. 1-5, Dec 2011.
[29] F. Adachi, M. Sawahashi, and H. Suda, "Wideband DS-CDMA for next-generation mobile communications systems," *Commun. Mag.*, vol. 36, no. 9, pp. 56-69, 1998.
[30] F. J. Harris, "On the Use of Windows for Harmonic Analysis with the Discrete Fourier Transform," in *Proc. IEEE*, vol. 66, no. 1, pp. 51-83, Jan. 1978.
[31] N. Yee and J. P. Linnartz, "Wiener filtering of multi-carrier CDMA in Rayleigh fading channel," in *Proc. 5th Int. Symp. IEEE Personal Indoor Mobile Radio Commun.*, vol. 4, pp. 1344-1347, Sep. 1994.
[32] J. Yu, Z. Jia, L. Yi, Y. Su, G.-K. Chang, and T. Wang, "Optical millimeter wave generation or up-conversion using external modulator," *IEEE Photon. Technol. Lett.*, vol. 18, no. 1, pp. 265-267, 2006.
[33] ITU-T Recommendation G.975.1, Appendix I.9, 2004.